Electrosynthesis of Biocompatible Free-Standing PEDOT Thin Films at a Polarised Liquid|Liquid Interface

Rob A. Lehane,[a,b,†] Alonso Gamero-Quijano,*[,a,b,†] Sigita Malijauskaite,[a,b] Angelika Holzinger,[a,b] Michelle Conroy,[a,c] Fathima Laffir,[a] Amit Kumar,[d] Ursel Bangert,[a,c] Kieran McGourty,[a,b,e] and Micheál D. Scanlon*[,a,b,f]

[a] Bernal Institute, University of Limerick (UL), Limerick V94 T9PX, Ireland

[b] Department of Chemical Sciences, School of Natural Sciences, University of Limerick (UL), Limerick V94 T9PX, Ireland

[c] Department of Physics, School of Natural Sciences, University of Limerick (UL), Limerick V94 T9PX, Ireland

[d] School of Mathematics and Physics, Queen's University Belfast (QUB), Belfast BT71 NN, UK

[e] Health Research Institute (HRI), University of Limerick (UL), Limerick V94 T9PX, Ireland

[f] The Advanced Materials and Bioengineering Research (AMBER) centre

[†] These authors contributed equally to the work.

* Corresponding author: daniel.gamero@ua.es

* Corresponding author: micheal.scanlon@ul.ie

Abstract

Conducting polymers (CPs) find applications in energy conversion and storage, sensor, and biomedical technologies, once processed into thin films. Hydrophobic CPs, like poly(3,4-ethylenedioxythiophene) (PEDOT), typically require surfactant additives, such as poly(styrenesulfonate) (PSS), to aid their aqueous processability as thin films. However, excess PSS diminishes CP electrochemical performance, biocompatibility, and device stability. Here, we report the electrosynthesis of PEDOT thin films at a polarised liquid|liquid interface, a method non-reliant on conductive solid substrates that produces free-standing, additive-free, biocompatible, easily transferrable, and scalable 2D PEDOT thin films of any shape or size in

a single-step at ambient conditions. Electrochemical control of thin film nucleation and growth at the polarised liquid|liquid interface allows control over the morphology, transitioning from 2D (flat on both sides with thickness <50 nm) to "Janus" 3D (with a flat and rough side, each showing distinct physical properties, and thickness >850 nm) films. The PEDOT thin films were *p*-doped (approaching the theoretical limit), showed high π-π conjugation, were processed directly as thin films without insulating PSS, and were thus highly conductive without post-processing. This work demonstrates that interfacial electrosynthesis directly produces PEDOT thin films with distinctive molecular architectures inaccessible in bulk solution or at solid electrode-electrolyte interfaces and emergent properties that facilitate technological advances. In this regard, we demonstrate the PEDOT thin film's superior biocompatibility as scaffolds for cellular growth, opening immediate applications in organic electrochemical transistor (OECT) devices for monitoring cell behaviour over extended time periods, bio-scaffolds and medical devices, without needing physiologically unstable and poorly biocompatible PSS.

Introduction

Conducting polymers (CPs) find widespread applications in energy conversion and storage, sensor, optoelectronic, photovoltaic, bioelectronic and biomedical technologies.[1–6] To satisfy this diverse set of applications, fabrication routes to CPs with desirable shapes/dimensions and compatibility with any substrate are required. The lightweight, flexible, and transparent nature of CPs makes them ideal for incorporation into technologies as thin films.[7]

Current methodologies to generate CP thin films have deficiencies that hinder technological progress. For example, multi-step film processing methods following chemical polymerisation require a complex of the CP and a hydrophilic surfactant, typically poly(styrenesulfonate) (PSS), to aid processability of technologically ubiquitous hydrophobic CPs, such as poly(3,4-ethylenedioxythiophene) (PEDOT).[8] However, excess PSS diminishes CP conductivity, long-term stability, specific capacity, and biocompatibility.[9–12] Electropolymerisation produces CP thin films in a single step,[13] but is limited to deposition onto conducting surfaces and less easily adapted to the synthesis of composite materials.[14] Vapour phase techniques are capable of producing CP thin films with record-high electrical conductivity,[15] but require high vacuum and/or temperatures, can be complicated or expensive to implement, and incompatible with heat-sensitive substrates.[16]

A liquid|liquid (L|L) interface provides a reproducible and defect-free environment to prepare and process free-standing two-dimensional (2D) thin films of nanomaterials, such as CPs, in a single step.[17] By polarising certain L|L interfaces, known as interfaces between two immiscible electrolyte solutions (ITIES),[18–20] exquisite electrochemical control over the kinetics of interfacial electron transfer (IET) between oxidant and monomer redox couples in opposite phases is achieved.

The groups of Cunnane, Mareček and Dryfe provided early insights into electrosynthesis of conducting polymers (CPs) at polarised aqueous|organic interfaces.[21–28] Cunnane first reported the electropolymerisation of short oligomer chains using 1-methylpyrrole and 1-phenylpyrrole monomers.[22] However, no interfacial thin film was formed with these relatively hydrophilic oligomers. Analysis of CP films formed with 2,2':5',2''-terthiophene showed poor electrochemical stability and conductivity,[24] likely due to over-oxidation of any CPs formed as the aqueous oxidant was consistently in significant excess over the monomer. Dryfe's group grew a polypyrrole film on single-walled carbon nanotubes at the interface during electropolymerisation.[28] However, the relatively hydrophilic pyrrole partitions to the aqueous phase, leading to uncontrolled chemical polymerisation in that phase. Electrosynthesis of Janus-Type gold/CP composites has been reported by Nishi *et al.* at a polarised L|L interface formed between a hydrophobic ionic liquid and water.[29] Up-scaling biphasic ionic liquid-based systems will be challenging due to their excessive viscosity and low conductivity.

In this work, we report a major advance in the use of interfacial electrosynthesis at an ITIES to prepare free-standing, additive-free, reproducible, easily transferrable, scalable, and biocompatible PEDOT thin films in a single step at optimised ambient conditions. The external electrochemical driving force, the interfacial Galvani potential difference ($\Delta_o^w\phi$), is applied using double potential step chronoamperometry (DPSCA). The IET reaction between an aqueous Ce^{4+} oxidant and organic EDOT monomer, and subsequent oligomer deposition at the L|L interface, can be assisted or hindered by manipulation of $\Delta_o^w\phi$. We demonstrate an emergent enhanced biocompatibility of free-standing PEDOT thin films prepared at the ITIES, compared with films prepared by drop-casting commercial PEDOT:PSS surfactant-free ink, using normal human retina pigment epithelium (hTERT RPE-1) cells. The latter are a physiologically pertinent cell line given the application of PEDOT films in maculopathies.[30,31] We functionally modified the PEDOT and PEDOT:PSS films through the incorporation of bioactive proteins and monitored the consequential effects on cell behaviour in each case.

These findings foreshadow potential applications as suitable 2D conductive substrates for RPE and electrically active photoreceptor cells and the development of organic electrochemical cell transistors (OECTs) capable of electrochemically monitoring cell growth over >24 hr periods.

Results and Discussion

The mechanism of PEDOT interfacial electrosynthesis. As illustrated in Figure 1a(i)-(v), PEDOT thin film interfacial electrosynthesis progresses along five distinct stages with time. Initially, IET occurs between the aqueous Ce^{4+} oxidant and EDOT organic monomer forming monomeric radical cations ($EDOT^{\bullet+}$) in the diffusion layer on the organic side of the ITIES (Figure 1a(i)). For IET to proceed with appreciable kinetics, the ITIES must be polarised positively, as detailed in Section S1 of the Supporting Information (SI) and discussed *vide infra*, with $\Delta_o^w\phi$ set to a value near the positive extreme of the Galvani polarisable potential window. $EDOT^{\bullet+}$ species are stabilised by the weakly coordinating organic anion, tetrakis(pentafluorophenyl)borate (TB^-),[32] and further couple with each other or EDOT monomers to form dimers in the diffusion layer. Continuous $EDOT^{\bullet+}$ generation by IET and ensuing radical coupling steps ultimately lead to the formation of EDOT oligomers that also coordinate with TB^- to maintain electroneutrality (Figure 1a(i)). The charge on the bulky TB^- anion is primarily centred on the boron atom.[33] Thus, weakly coordinating TB^- has a poor ability to compensate the positive charge on the cationic EDOT oligomers which consequently maintain a net positive charge. The radical coupling steps also result in the release of protons on the organic side of the ITIES (see Section S2, SI, and Figure S1) that will be stabilised by the PEDOT thin film itself or by water present inside the film.[34]
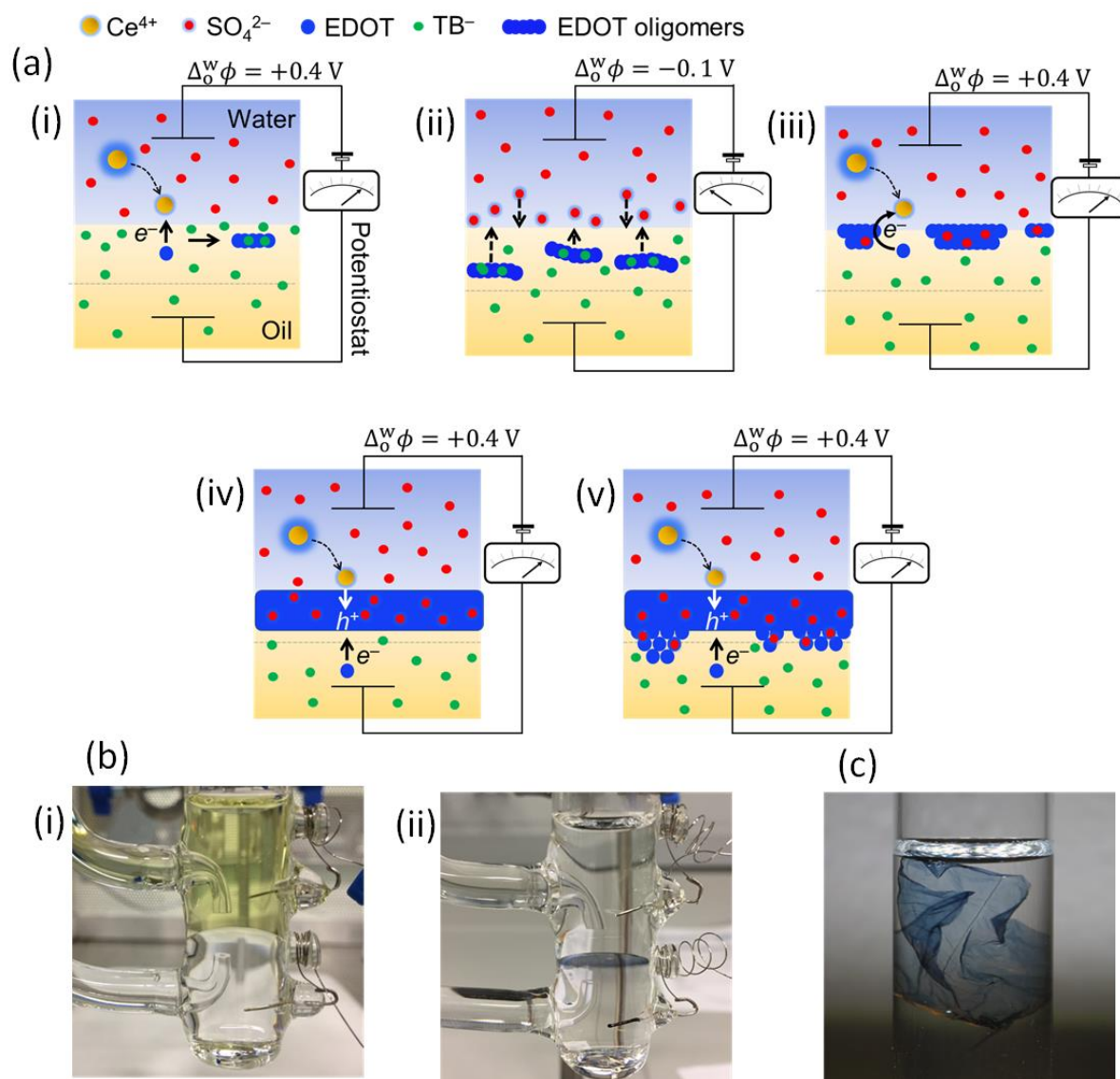
Figure 1. The mechanism of PEDOT interfacial electrosynthesis at the interface between two immiscible electrolyte solutions (ITIES). (a) The mechanism is schematically shown as five distinct steps with time: **(i)** interfacial electron transfer (IET) at a positive externally applied interfacial Galvani potential difference ($\Delta_o^w \phi = +0.4$ V) between the aqueous Ce^{4+} oxidant and organic EDOT monomer to form cationic EDOT oligomers, **(ii)** interfacial adsorption of the cationic EDOT oligomers at a more negative $\Delta_o^w \phi$ (= –0.1 V) through an ion-pairing and interchange interaction with the aqueous SO_4^{2-} anions, **(iii)** autocatalytic IET between Ce^{4+} and EDOT at adsorbed EDOT oligomer sites that act as interfacial bipolar electrodes, **(iv)** adsorbed EDOT oligomer coalescence to form a highly compact 2D PEDOT thin film at the ITIES that is flat on both sides and heavily doped with aqueous SO_4^{2-} anions, and **(v)** continued IET leading to a secondary growth process into the organic phase and the formation of a porous 3D structure on the organic-facing side as the thickness of the PEDOT thin film increases. **(b)** The four-electrode electrochemical cell **(i)** before and **(ii)** after interfacial electrosynthesis. The acidic aqueous phase, containing the yellow Ce^{4+} oxidant, is on top and the more dense α, α, α-trifluorotoluene (TFT) organic solution containing the EDOT monomer is on the bottom. PEDOT forms exclusively as a thin blue film at the polarised liquid|liquid (L|L) interface. **(c)** A PEDOT thin film removed from a large ITIES and stored in an acetone/0.2 M H_2SO_4 mixture to minimise gradual undoping

Interfacial adsorption involving ion-pairing and interchange between the cationic EDOT oligomers and aqueous electrolyte anions (herein SO_4^{2-}) takes place once the oligomers reach a critical size after an induction period (Figure 1a(ii)). SO_4^{2-} anions displace the weakly coordinating organic TB^- anions during interfacial adsorption, ultimately becoming the sole dopant anion in the PEDOT thin film. This deposition process is driven by the energetically favourable reduction of the interfacial tension (γ) between the two repulsive phases upon oligomer adsorption.[35] Setting $\Delta_o^w\phi$ slightly negative of the potential of zero charge (PZC) is optimal for oligomer adsorption, ensuring the presence of a sufficient concentration of SO_4^{2-} at the L|L interface to participate in ion-pairing. Thus, as the IET and oligomer interfacial adsorption steps take place at different applied $\Delta_o^w\phi$, potentiodynamic or multi-step potentiostatic are favoured over single-step potentiostatic electrochemical techniques. Also, a negative $\Delta_o^w\phi$ will facilitate the pumping of protons, generated on the organic side of the ITIES during the IET/radical coupling process at a positive $\Delta_o^w\phi$, to the aqueous phase *via* either direct ion transfer or the Grotthuss mechanism through the PEDOT thin film (Figure S2).

In the next step, nucleation and growth of adsorbed EDOT oligomers takes place at the interface. The EDOT oligomers act as floating interfacial bipolar electrodes, providing abundant catalytic sites as electrical short-cuts to catalyse IET between the Ce^{4+} and EDOT species (Figure 1a(iii)).[36–38] Due to this autocatalytic effect, IET proceeds at a much lower overpotential than at a bare ITIES, with a higher kinetic rate. Thus, the PEDOT islands show rapid 2D growth, parallel to the L|L interface. The gaps between individual rapidly growing islands of PEDOT disappear and a highly compact 2D PEDOT thin film coalesces at the ITIES that is flat on both sides, with a thickness of ~50 nm (Figure 1a(iv)). At this point, a physical barrier now exists between the Ce^{4+} and EDOT species at the ITIES. However, IET continues through the conductive PEDOT thin film and is subject to the influence of the diffusion of SO_4^{2-} counter-anions through the film to maintain electroneutrality locally, *i.e., "p*-doping". At this point, after the PEDOT thin film has coated the interface, the mechanism of SO_4^{2-} doping can be considered analogous to facilitated ion transfer (FIT) at the polarised L|L interface, specifically the transfer by interfacial complexation (TIC) mechanism.[39–41] Continued IET initiates a secondary 3D growth process into the organic phase as the thickness of the PEDOT thin film increases. This controllable secondary growth process leads to the formation of a highly porous 3D structure, up to ~ 850 nm thick (Figure 1a(v)).

Electrochemically initiating and controlling PEDOT thin film interfacial electrosynthesis. IET between Ce^{4+} and EDOT leading to a 2D PEDOT thin film is not a spontaneous process at an aqueous|α, α, α-trifluorotoluene (TFT) interface (Figure S3). To initiate CP thin film formation, the aqueous|TFT interface must be polarised using a potentiostat in conjunction with a four-electrode electrochemical cell (Figure 1b and Figure S4). The resulting free-standing 2D PEDOT thin film could be recovered from the L|L interface, washed with acetone and suspended in an acetone:sulfuric acid mixture (Figure 1c) for storage before *ex situ* characterisation or applications. Optimal conditions for thin film formation required a low concentration of oxidant (with the monomer always in excess), which is unconventional in chemical synthesis. A thermodynamic analysis of this biphasic system explains the need for an external electrochemical driving force to drive interfacial electrosynthesis with significant kinetics (Section S3, SI).

Double potential step chronoamperometry (DPSCA) cycling provided the external driving force, with the four-electrode electrochemical cell configuration outlined in Figure 2a. Current-time transients for the initial six DPSCA cycles are shown in Figure 2b. A single DPSCA cycle involves first holding $\Delta_o^w \phi$ at +0.4 V for 10 s to induce IET between Ce^{4+} and EDOT with appreciable kinetics, leading to a positive current-time transient and the formation of cationic EDOT oligomers in the diffusion zone on the organic side of the ITIES. Next, $\Delta_o^w \phi$ is held at –0.1 V for a further 10 s to induce EDOT oligomer interfacial adsorption, leading to a negative current-time transient. The value of –0.1 V was chosen as it is slightly negative of the PZC at a bare aqueous|TFT interface, determined as ca. 0 V by AC voltammetry (Figure 2c), and optimal for oligomer adsorption as discussed *vide supra*. After 50 DPSCA cycles, a blue PEDOT thin film becomes visible at the aqueous|TFT interface (Figure 1b(ii)).
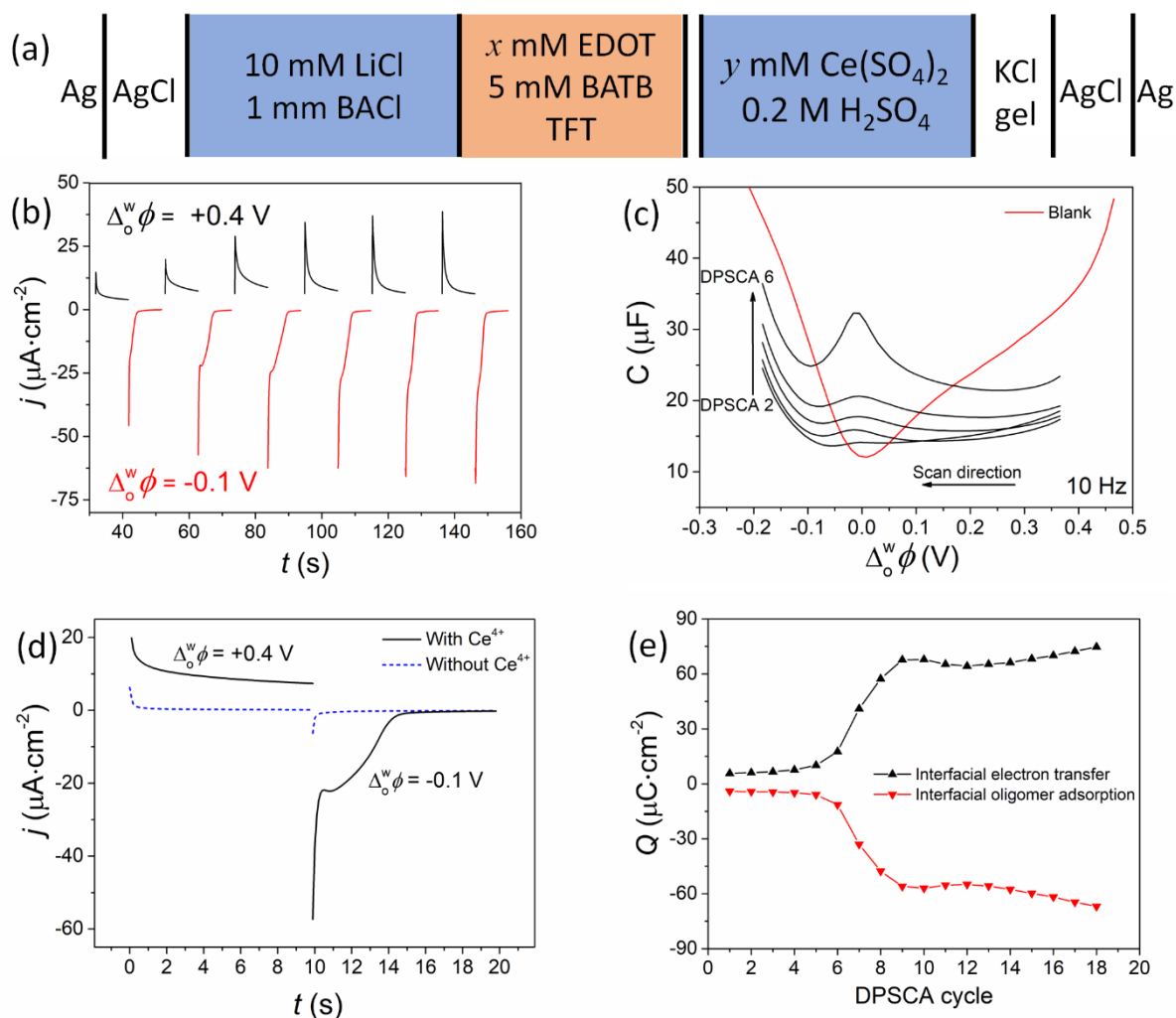
Figure 2. Electrochemically initiating, controlling, and monitoring PEDOT thin film interfacial electrosynthesis. (a) Electrochemical cell configuration of the four-electrode electrochemical cell employed. For blank experiments x and y are both 0 mM. For interfacial electrosynthesis experiments x and y are 5 and 2 mM, respectively. In this four-electrode configuration, the organic Pt and Ag/AgCl electrodes were connected to the counter and reference terminals, respectively, while the aqueous Pt and Ag/AgCl electrodes were connected to the working and sensing terminals, respectively. All experiments were carried out under aerobic conditions. (b) Current-time transients recorded during double potential step chronoamperometry (DPSCA) cycles 5 to 10 in the presence of aqueous Ce^{4+} and organic EDOT. The first potential step was held at $\Delta_o^w\phi = +0.4$ V for 10 s, and the second at $\Delta_o^w\phi = -0.1$ V for 10 s. (c) Differential capacitance (C / μF) measurements performed at a bare aqueous|TFT interface (red line) and after DPSCA cycles 2 to 6 (black lines) in the presence of aqueous Ce^{4+} and organic EDOT. The frequency was 10 Hz, the amplitude was 10 mV and the scan direction was from positive to negative potential. (d) Control DPSCA experiments. Current-time transients recorded during a DPSCA cycle with (black lines) and without (dashed blue lines) the aqueous Ce^{4+} oxidation present during PEDOT interfacial electrosynthesis. (e) Plot of the charge (Q / μC·cm^{-2}) for each potential step recorded for the first 18 DPSCA cycles. All electrochemical experiments were performed using the cell configuration outlined in Figure 2a under aerobic conditions

No change in charge was observed after 100 DPSCA cycles during control experiments without Ce^{4+} present (Figure 2d). Trends in the kinetics of interfacial electrosynthesis with DPSCA cycle number were determined by analysing the charge magnitudes recorded from both the positive and negative current transients during the first 18 DPSCA cycles (Figure 2e). These trends corroborated the mechanism outlined in Figure 1a, as detailed in Section S4.1, SI.

Evidence of interfacial ion-pairing and interchange between adsorbed EDOT oligomers and SO_4^{2-} anions during interfacial electrosynthesis is provided by comparison of differential capacitance measurements of the blank aqueous|TFT interface and after DPSCA cycles 2 to 6 in the presence of Ce^{4+} and EDOT (Figure 2c and Section S4.2, SI). *In situ* parallel-beam UV/vis absorbance measurements show the depletion of Ce^{4+} on the aqueous side of the L|L interface with continuous DPSCA cycling and PEDOT thin film formation at the ITIES after 300 DPSCA cycles (Figure S11).

Although hydrophobic, the EDOT monomer is slightly soluble in aqueous solutions. Therefore, it is expected that a quantity of the EDOT monomer (and indeed low molecular weight EDOT oligomers) will partition across the L|L interface during the initial stages of the electrosynthesis. This is evident from the strong Tyndall effect seen in the aqueous phase after interfacial electrosynthesis (Figure S12) due to the presence of EDOT oligomers. Definitively distinguishing a "truly heterogeneous IET" mechanism from an "interfacial partition followed by homogeneous ET" mechanism experimentally at a polarised L|L interface is difficult.[42] As a result, we cannot decisively conclude that the initial IET reaction between Ce^{4+} and the EDOT monomer is truly heterogeneous (shown in Figure 1(a)(i)). Nevertheless, partitioned EDOT oligomeric species suspended in the aqueous phase are not likely to be involved in the formation of the PEDOT thin film at the L|L interface, as discussed in Section 4.4, SI.

Potentiostatic experiments holding $\Delta_o^w \phi$ at +0.4 V for 1,000 s were also studied (Figure S13). In this case, the quantity of cationic EDOT oligomer adsorption was minimal due to aqueous SO_4^{2-} anions being unavailable to undergo ion-pairing at +0.4 V at the L|L interface. Furthermore, oligomer adsorption is a balance between the interfacial tension (γ) and the oligomer size. Therefore, factors that lower γ, such as applied potentials close to the positive or negative ends of the polarisable potential window,[43] may slow the adsorption kinetics as the oligomers "critical size" increases. Nevertheless, after 1,000 s, a PEDOT thin film could be seen coating the L|L interface. However, this thin film was not mechanically robust enough to recover for *ex situ* characterisation in comparison to films prepared by DPSCA.

Microscopic analysis. Scanning electron microscopy (SEM) of a 2D PEDOT thin film prepared by DPSCA (150 cycles) revealed an asymmetric "Janus" morphology (see Figure 3a, Section S5, SI, and Figure S14). One side is flat and featureless at the nanoscale, while the other shows a rough, porous 3D structure. The PEDOT thin films adhere to any solid substrate, with the thin film closely following the contours and taking the shape of the surface (Figures S15 and S16). The asymmetric nature of the PEDOT thin film leads to each side having distinct physical properties. For example, sessile drop measurements highlight significant differences in hydrophobicity, with water droplet contact angles of 89.5^{o} and 112.6^{o} measured on the flat and rough sides, respectively (Figure 3b). Atomic force microscopy (AFM) images of the topography of a PEDOT thin film folded back on itself clearly highlight the differences in surface roughness of either side (Figure 3c(i)) and revealed that the thickness of a thin film prepared by 50 DPSCA cycles is ca. 60 nm (Figure 3c(ii)-(iii)).
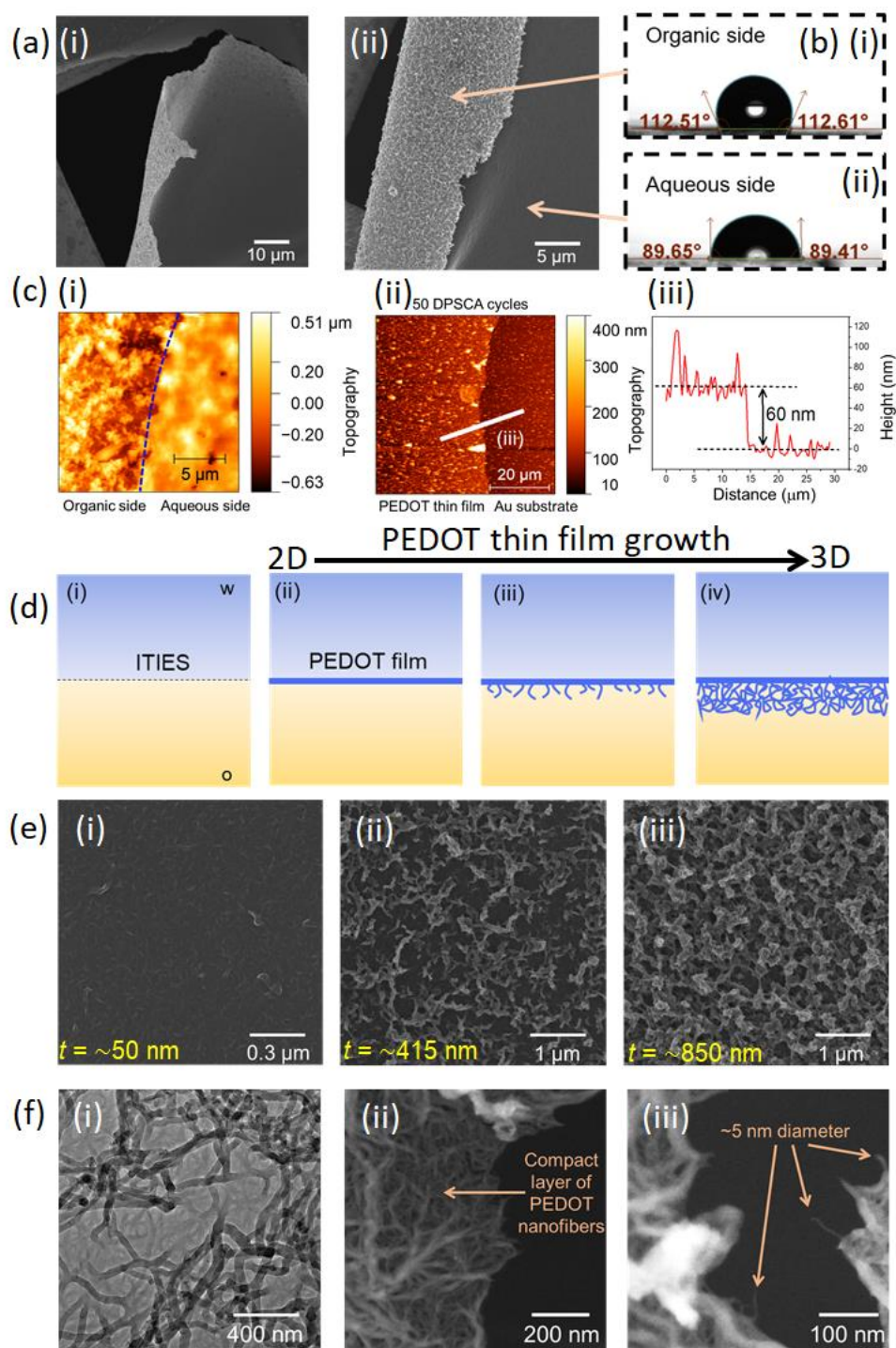
Figure 3. Microscopic analysis of the PEDOT thin film. (a) Scanning electron microscopy (SEM) images of a free-standing 2D PEDOT film electrosynthesised at the ITIES, showing the distinct morphologies of the "smooth" aqueous facing side and "rough" organic facing side. Additional SEM images are provided in Section S5.1, SI. **(b)** Sessile drop contact angle measurements recorded on each side of the PEDOT thin film, highlighting the influence of the morphology on the measured hydrophobicity. **(c)** Atomic force microscopy (AFM) analysis of **(i)** the topography of a PEDOT thin film folded back on itself and **(ii), (iii)** the thickness of a PEDOT thin film on a flat gold substrate after 50 DPSCA cycles. **(d)** Schematic of the different stages of PEDOT thin film growth, from 2D to 3D, as a function of continued DPSCA cycling. **(e)** SEM images showing the organic facing side of the PEDOT thin film, demonstrating the

controllable growth on the organic facing side of the thin film from 2D to 3D as a function of DPSCA cycling. The thickness (t) of each thin film was determined by AFM (Figure S17). **(f) (i)** Bright field and **(ii), (iii)** dark field mode transmission electron microscopy (TEM) imaging shows that the film is a compact network of PEDOT nanofibers that have a diameter that ranges from < 5 nm up to 50 nm. The arrows in (iii) point to PEDOT nanofibers with a diameter of ca. 5 nm. All PEDOT thin films analysed were prepared by DPSCA cycling using the cell configuration outlined in Figure 2a.

The evolution of the morphology of the organic facing side of the PEDOT thin film with DPSCA cycling is depicted schematically in Figure 3d(i)-(iv), with SEM images of each stage provided (Figure 3e(i)-(iii)) and the thickness of each stage determined by AFM (Figure S17). Initially, after 50 DPSCA cycles, the thin film shows 2D growth parallel to the ITIES, a highly compact structure that is flat on both sides, and a thickness of 40 – 60 nm (Figure 3e(i)). With continued interfacial electrosynthesis (up to 150 DPSCA cycles), secondary 3D growth begins to extend into the organic phase as the thickness of the PEDOT thin film increases (Figure 3e(ii)). This controllable secondary growth process leads to the formation of a very porous 3D structure with a thickness of up to ~ 850 nm after prolonged (> 300 DPSCA cycles) interfacial electrosynthesis (Figure 3e(iii)).

Transmission electron microscopy (TEM) studies revealed that the PEDOT thin film is exceptionally stable under the TEM beam (80 kV), signalling a high thermal conductivity and providing an opportunity to further investigate the PEDOT thin film's nanostructure. Both bright-field (Figure 3f(i)) and dark-field (Figure 3f(ii)-(iii)) mode TEM images show that the flat aqueous side consists of a compact layer of PEDOT nanofibers that run parallel to the ITIES. The diameter of the PEDOT nanofibers varies from < 5 nm to above 50 nm. We propose that the nanofibers with a diameter of < 5 nm are first to be deposited at the ITIES during interfacial electrosynthesis, forming an initial compact layer. Subsequently, the nanofiber diameter increases as the thin film grows down into the organic phase.

Spectroscopic, conductivity and electrochemical analysis. *Ex situ* spectroscopic analysis was performed on PEDOT thin films transferred to suitable solid substrates (Section S6, SI). A bipolaron band was observed by UV/vis absorbance, signifying that the PEDOT thin film is in an oxidised state[44] and *p*-doped (Figure S18). Raman spectroscopy also confirmed that the PEDOT thin film is *p*-doped, with high π-π conjugation and a benzenoid (coiled) configuration to the polymer chain (Figure S19), the more stable form when PEDOT is highly doped.[45–47] An X-ray-photoelectron spectroscopy (XPS) survey spectrum showed the presence of only sulfur, carbon and oxygen (Figure S20), indicating that the cerium oxidant, boron and

fluorine are not incorporated into the thin film. This implies that the organic TB$^-$ anion is not involved in p-doping and SO$_4^{2-}$ is the primary dopant. Further XPS analysis revealed that the doping level was estimated as ~39% (Figure S21), in line with previous reports of the upper limits possible of PEDOT doping between 35 – 40%.[48,49]

Excess negative charge from the insulating surfactant PSS can detrimentally alter the conduction mechanism of CP thins films,[50] for more details see Section S7.1, SI. *Ex situ* conductivity of the PEDOT thin film was determined as 554 ($\pm$77) S·cm^{-1} (Section S7.2, SI, and Figure S22), comparable to the highest conductivity value reported for a pristine PEDOT:ClO$_4^-$ film (400–650 S·cm^{-1}) made by conventional electropolymerisation at a solid electrode surface in acetonitrile.[51,52] The *in situ* conductivity of a PEDOT thin film and a commercial PEDOT:PSS film drop cast and annealed directly onto a microelectrode array were compared in PBS buffer solution (Figure S23). The PEDOT and PEDOT:PSS films had maximum conductivities of ~5.35 S·cm^{-1} and ~1.2 S·cm^{-1}, respectively, in their plateau regions, with the conductance window in the PEDOT thin film 0.4 V greater than that of the PEDOT:PSS film (Figure S24). The latter is advantageous for OECT devices working at lower potentials to avoid oxidative reactions or biological stress (if the active layer is to be functionalised with cells). Corresponding CVs of each film in PBS buffer solution were obtained using a range of scan rates and potential ranges (Figures S25 and S26). The PEDOT thin film remains doped over a very wide potential range (in comparison to the PEDOT:PSS film) and therefore has high conductivity even at negative potentials. At high scan rates, the PEDOT thin film displays an ideal capacitive behaviour due to the polymer films high intrinsic conductivity and wide conductance window.

Biocompatibility studies. PEDOT:PSS films are being extensively explored for the treatment of visual impairment, particularly relating to amelioration or restoration of retinal function.[30,31] However, the action of PSS severely hampers the biocompatibility and integrity of the resultant implantable biodevices (Section S8.2, SI). In this context, the biocompatibility of PEDOT thin films electrosynthesised at the ITIES was compared with that of a drop cast PEDOT:PSS film using an adherent cell line derived from normal human retina pigment epithelium (hTERT RPE-1), see Figure 4.

Following 48 hours of cell growth on each film, marked differences were observed in hTERT RPE-1 cell growth dynamics (Figure 4). Overall, in the presence of PEDOT thin films, cells exhibited a greater degree of proliferation and showed a stretched morphology, associated with actin bundle stress fibre formation, alluding to the more biocompatible nature of PEDOT

versus PEDOT:PSS (Figure 4a-b). These data re-enforce the challenges of using PSS at bio-interfaces and differentiate our investigations from many evaluating PEDOT:PSS in cell culture, where lack of obvious cytotoxicity is incorrectly construed as high biocompatibility. Next, each film was evaluated for suitability of active biomolecule incorporation. Collagen was selected as an active biomolecule due to its known influence on cell proliferation and adhesion, which could potentially mitigate the poor cellular growth seen on PEDOT:PSS samples. While only marginal effects were observed in cells grown on PEDOT:PSS films, functionalisation of PEDOT thin films resulted in a marked amplification in cell proliferation and cell spreading, indicative of robust adhesion receptor engagement and bioactivation of the cell cycle programme (Fig 4a).
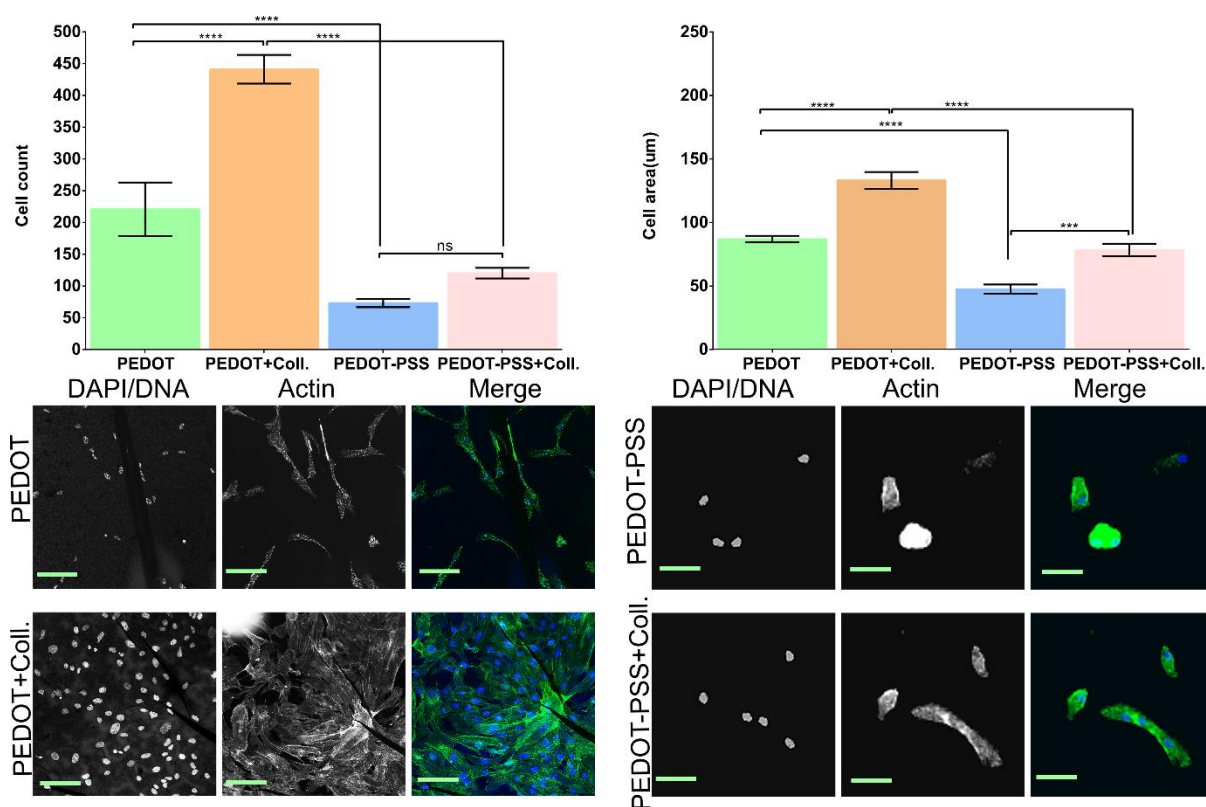
Figure 4. Biocompatibility of PEDOT thin films prepared at the ITIES and drop-cast PEDOT:PSS films with and without collagen functionalisation. **(a)** Cell proliferation analysis **(b)** Cell area analysis for each sample film. Scale bar represents 50 µm.

Conclusions

Interfacial electrosynthesis bridges the fields of purely homogeneous (chemical) electron transfer reactions between redox couples, which are difficult to control, and finely

controlled (electrochemical) heterogeneous electron transfer at conventional solid electrode-electrolyte interfaces. Polarising the L|L interface provides an in-built ability to control the kinetics of IET between oxidant and monomer redox couples in opposite phases and probe the mechanism *in situ* electrochemically. These two features elevate this work over studies that involve spontaneous interfacial reactions (polycondensation, polyaddition, self-assembly),[53–56] that permit only rudimentary chemical control over reaction kinetics and a limited ability to study the synthetic mechanism *in situ*. Our work unravels the underlying thermodynamic limitations and mechanism of PEDOT thin film interfacial electrosynthesis that progresses along five distinct stages with time. This underlying mechanism will be broadly generic for all aqueous oxidant/organic monomer combinations that are thermodynamically compatible to facilitate IET within the Galvani polarisable potential window (where the IET kinetics are under direct external electrochemical control). Such an understanding will allow us to identify suitable oxidant/monomer combinations, opening the field of interfacial electrosynthesis to other technologically critical CPs beyond PEDOT, *e.g.,* poly(3-hexylthiophene-2,5-diyl), commonly known as P3HT.

The PEDOT thin films prepared by interfacial electrosynthesis showed superior biocompatibility and suitability to be used as a scaffold for cellular growth without the need for further modification designed to promote cell adhesion or enhance viability. Bioactive molecules can be readily incorporated into PEDOT polymers as a further customisable parameter for cell growth studies. This opens an attractive avenue for potential new and improved OECT devices for monitoring cell behaviour over extended time periods, bio-scaffolds and medical devices, without the requirement for physiologically unstable and poorly biocompatible PSS. The dimensions and geometry of free-standing thin films possible by interfacial electrosynthesis are only limited by the interfacial area and shape defined by the electrochemical cell. Furthermore, we demonstrate that interfacial electrosynthesis is a local and mild process that requires minimal reagents (*e.g.,* low oxidant concentrations) and is thus highly compatible with large scale thin film production. In this regard, future work will explore polarising the L|L interface chemically, by establishing a suitable distribution potential through ion partition between the two phases, to scale-up thin film production.

Associated Content

Supporting information

Supplementary materials and methods. Supplementary sections detailing the mechanism and thermodynamics of PEDOT interfacial electrosynthesis. Supplementary section detailing the electrochemical initiation, control, and monitoring of PEDOT interfacial electrosynthesis. Supplementary figures and discussions describing the microscopic (SEM, TEM), spectroscopic (UV/vis, Raman, XPS), conductivity and electrochemical properties of the PEDOT thin films. Supplementary details of the biocompatibility studies using PEDOT thin films.

Author Information

Corresponding Authors

* daniel.gamero@ua.es (A. Gamero-Quijano)

* micheal.scanlon@ul.ie (M.D. Scanlon)

ORCID IDs

Rob A. Lehane: 0000-0001-6478-3030

Alonso Gamero-Quijano: 0000-0002-7173-2861

Sigita Malijauskaite: 0000-0001-7810-6305

Angelika Holzinger: 0000-0003-1661-830X

Michele Conroy: 0000-0002-6658-1819

Fathima Laffir: n/a

Amit Kumar: 0000-0002-1194-5531

Ursel Bangert: 0000-0002-7511-7663

Kieran McGourty: 0000-0003-1218-1833

Micheál D. Scanlon: 0000-0001-7951-7085

Notes
The authors declare no competing financial interest.

Author Contributions

The authors R.A.L and A.G.-Q. contributed equally to the work.

Acknowledgements

References

(1)   Huang, J.; Virji, S.; Weiller, B. H.; Kaner, R. B. Polyaniline Nanofibers: Facile Synthesis and Chemical Sensors. *J. Am. Chem. Soc.* **2003**, *125* (2), 314–315. https://doi.org/10.1021/ja028371y.

(2)   Xia, Y.; Sun, K.; Ouyang, J. Solution-Processed Metallic Conducting Polymer Films as Transparent Electrode of Optoelectronic Devices. *Adv. Mater.* **2012**, *24* (18), 2436–2440. https://doi.org/10.1002/adma.201104795.

(3)   Ghosh, S.; Maiyalagan, T.; Basu, R. N. Nanostructured Conducting Polymers for Energy Applications: Towards a Sustainable Platform. *Nanoscale* **2016**, *8* (13), 6921–6947. https://doi.org/10.1039/c5nr08803h.

(4)   Someya, T.; Bao, Z.; Malliaras, G. G. The Rise of Plastic Bioelectronics. *Nature* **2016**, *540* (7633), 379–385. https://doi.org/10.1038/nature21004.

(5)   Zhang, Y.; Ng, S. W.; Lu, X.; Zheng, Z. Solution-Processed Transparent Electrodes for Emerging Thin-Film Solar Cells. *Chem. Rev.* **2020**, *120* (4), 2049–2122. https://doi.org/10.1021/acs.chemrev.9b00483.

(6)   Sultana, N.; Chang, H. C.; Jefferson, S.; Daniels, D. E. Application of Conductive Poly(3,4-Ethylenedioxythiophene):Poly(Styrenesulfonate) (PEDOT:PSS) Polymers in Potential Biomedical Engineering. *Journal of Pharmaceutical Investigation*. Springer Singapore 2020, pp 437–444. https://doi.org/10.1007/s40005-020-00485-w.

(7)   D'Arcy, J. M.; Tran, H. D.; Tung, V. C.; Tucker-Schwartz, A. K.; Wong, R. P.; Yang, Y.; Kaner, R. B. Versatile Solution for Growing Thin Films of Conducting Polymers. *Proc. Natl. Acad. Sci. U. S. A.* **2010**, *107* (46), 19673–19678. https://doi.org/10.1073/pnas.1008595107.

(8)   Yang, Y.; Deng, H.; Fu, Q. Recent Progress on PEDOT:PSS Based Polymer Blends and Composites for Flexible Electronics and Thermoelectric Devices. *Mater. Chem. Front.* **2020**, *4* (11), 3130–3152. https://doi.org/10.1039/d0qm00308e.

(9)   Spencer, A. R.; Primbetova, A.; Koppes, A. N.; Koppes, R. A.; Fenniri, H.; Annabi, N. Electroconductive Gelatin Methacryloyl-PEDOT:PSS Composite Hydrogels: Design, Synthesis, and Properties. *ACS Biomater. Sci. Eng.* **2018**, *4* (5), 1558–1567. https://doi.org/10.1021/acsbiomaterials.8b00135.

(10)   Cameron, J.; Skabara, P. J. The Damaging Effects of the Acidity in PEDOT:PSS on Semiconductor Device Performance and Solutions Based on Non-Acidic Alternatives. *Mater. Horizons* **2020**, *7* (7), 1759–1772. https://doi.org/10.1039/c9mh01978b.

(11)   Grossiord, N.; Kroon, J. M.; Andriessen, R.; Blom, P. W. M. Degradation Mechanisms in Organic Photovoltaic Devices. *Org. Electron.* **2012**, *13* (3), 432–456. https://doi.org/10.1016/j.orgel.2011.11.027.

(12)   Stöcker, T.; Köhler, A.; Moos, R. Why Does the Electrical Conductivity in PEDOT:PSS Decrease with PSS Content? A Study Combining Thermoelectric Measurements with Impedance Spectroscopy. *J. Polym. Sci. Part B Polym. Phys.* **2012**, *50* (14), 976–983. https://doi.org/10.1002/polb.23089.

(13)   Zhou, M.; Heinze, J. Electropolymerization of Pyrrole and Electrochemical Study of Polypyrrole: 1. Evidence for Structural Diversity of Polypyrrole. *Electrochim. Acta* **1999**, *44* (11), 1733–1748. https://doi.org/10.1016/S0013-4686(98)00293-X.

(14)   Reynolds, J. R.; Thompson, B. C.; Skotheim, T. A. *Conjugated Polymers: Properties, Processing, and Applications*; CRC Press, 2019, 2019.

(15)   Wang, X.; Lee, S.; Wang, M.; Zhao, J.; Zhang, X.; Sun, L.; Shao-Horn, Y.; Dincă, M.; Lee, D.; Gleason, K. K.; Palacios, T. High Electrical Conductivity and Carrier Mobility in OCVD PEDOT Thin Films by Engineered Crystallization and Acid Treatment. *Sci. Adv.* **2018**, *4* (9), eaat5780. https://doi.org/10.1126/sciadv.aat5780.

(16)   Evans, D.; Fabretto, M.; Mueller, M.; Zuber, K.; Short, R.; Murphy, P. Structure-Directed Growth of High Conductivity PEDOT from Liquid-like Oxidant Layers during Vacuum Vapor Phase Polymerization. *J. Mater. Chem.* **2012**, *22* (30), 14889–14895. https://doi.org/10.1039/c2jm32281a.

(17)   Zarbin, A. J. G. Liquid-Liquid Interfaces: A Unique and Advantageous Environment to Prepare and Process Thin Films of Complex Materials. *Mater. Horizons* **2021**, *8* (5), 1409–1432. https://doi.org/10.1039/d0mh01676d.

(18)   Suárez-Herrera, M. F.; Scanlon, M. D. On the Non-Ideal Behaviour of Polarised Liquid-Liquid Interfaces. *Electrochim. Acta* **2019**, *328*, 1–9. https://doi.org/10.1016/j.electacta.2019.135110.

(19)   Gschwend, G. C.; Olaya, A.; Peljo, P.; Girault, H. H. Structure and Reactivity of the Polarised Liquid–Liquid Interface: What We Know and What We Do Not. *Curr. Opin. Electrochem.* **2020**, *19*, 137–143. https://doi.org/10.1016/j.coelec.2019.12.002.

(20)   Samec, Z. Electrochemistry at the Interface between Two Immiscible Electrolyte Solutions (IUPAC Technical Report). *Pure Appl. Chem.* **2004**, *76* (12), 2147–2180. https://doi.org/10.1351/pac200476122147.

(21)   Maeda, K.; Jänchenová, H.; Lhotský, A.; Stibor, I.; Budka, J.; Mareček, V. Formation of a Polymer Layer from Monomers Adsorbed at a Liquid|liquid Interface. *J. Electroanal. Chem.* **2001**, *516* (1–2), 103–109. https://doi.org/10.1016/S0022-0728(01)00658-1.

(22)   Cunnane, V. J.; Evans, U. Formation of Oligomers of Methyl- and Phenyl-Pyrrole at an Electrified Liquid/Liquid Interface. *Chem. Commun.* **1998**, No. 19, 2163–2164. https://doi.org/10.1039/a806365f.

(23)   Johans, C.; Clohessy, J.; Fantini, S.; Kontturi, K.; Cunnane, V. J. Electrosynthesis of Polyphenylpyrrole Coated Silver Particles at a Liquid-Liquid Interface. *Electrochem. commun.* **2002**, *4* (3), 227–230. https://doi.org/10.1016/S1388-2481(02)00256-4.

(24)   Gorgy, K.; Fusalba, F.; Evans, U.; Kontturi, K.; Cunnane, V. J. Electropolymerization of 2,2′:5′,2″ Terthiophene at an Electrified Liquid-Liquid Interface. *Synth. Met.* **2002**, *125* (3), 365–373. https://doi.org/10.1016/S0379-6779(01)00474-X.

(25)   Evans-Kennedy, U.; Clohessy, J.; Cunnane, V. J. Spectroelectrochemical Study f 2,2':5',2''-Terthiophene Polymerization at a Liquid / Liquid Interface Controlled by Potential-Determining Ions. *Macromolecules* **2004**, *37*, 3630–3634.

(26)   Vignali, M.; Edwards, R.; Cunnane, V. J. Characterization of Doping and Electropolymerization of Free Standing Films of Polyterthiophene. *J. Electroanal. Chem.* **2006**, *592* (1), 37–45. https://doi.org/10.1016/j.jelechem.2006.04.020.

(27)   Vignali, M.; Edwards, R. A. H.; Serantoni, M.; Cunnane, V. J. Electropolymerized Polythiophene Layer Extracted from the Interface between Two Immiscible Electrolyte Solutions: Current-Time Analysis. *J. Electroanal. Chem.* **2006**, *591* (1), 59–68. https://doi.org/10.1016/j.jelechem.2006.03.033.

(28)   Toth, P. S.; Rabiu, A. K.; Dryfe, R. A. W. Controlled Preparation of Carbon Nanotube-Conducting Polymer Composites at the Polarisable Organic/Water Interface. *Electrochem. commun.* **2015**, *60*, 153–157. https://doi.org/10.1016/j.elecom.2015.08.022.

(29)   Nishi, N.; Yajima, I.; Amano, K. I.; Sakka, T. Janus-Type Gold/Polythiophene Composites Formed via Redox Reaction at the Ionic Liquid|Water Interface. *Langmuir* **2018**, *34* (7), 2441–2447. https://doi.org/10.1021/acs.langmuir.7b03792.

(30)   Maya-Vetencourt, J. F.; Ghezzi, D.; Antognazza, M. R.; Colombo, E.; Mete, M.; Feyen, P.; Desii, A.; Buschiazzo, A.; Di Paolo, M.; Di Marco, S.; Ticconi, F.; Emionite, L.; Shmal, D.; Marini, C.; Donelli, I.; Freddi, G.; MacCarone, R.; Bisti, S.; Sambuceti, G.; Pertile, G.; Lanzani, G.; Benfenati, F. A Fully Organic Retinal Prosthesis Restores Vision in a Rat Model of Degenerative Blindness. *Nat. Mater.* **2017**, *16* (6), 681–689. https://doi.org/10.1038/nmat4874.

(31)   Ferlauto, L.; Airaghi Leccardi, M. J. I.; Chenais, N. A. L.; Gilliéron, S. C. A.; Vagni, P.; Bevilacqua, M.; Wolfensberger, T. J.; Sivula, K.; Ghezzi, D. Design and Validation of a Foldable and Photovoltaic Wide-Field Epiretinal Prosthesis. *Nat. Commun.* **2018**, *9* (1), 1–15. https://doi.org/10.1038/s41467-018-03386-7.

(32)   Kobayashi, H. Weakly Coordinating Bulky Anions Designed by Efficient Use of Polyfluoro-Substitution. *J. Fluor. Chem.* **2000**, *105* (2), 201–203. https://doi.org/10.1016/S0022-1139(00)00274-8.

(33)   Andreeva, N. A.; Chaban, V. V. Understanding Weakly Coordinating Anions: Tetrakis(Pentafluorophenyl)Borate Paired with Inorganic and Organic Cations. *J. Mol. Model.* **2017**, *23* (3), 86. https://doi.org/10.1007/s00894-017-3275-2.

(34)   He, S.; Mukaida, M.; Kirihara, K.; Lyu, L.; Wei, Q. Reversible Protonic Doping in Poly(3,4-Ethylenedioxythiophene). *Polymers (Basel).* **2018**, *10* (10). https://doi.org/10.3390/polym10101065.

(35)   Johans, C.; Lahtinen, R.; Kontturi, K.; Schiffrin, D. J. Nucleation at Liquid|liquid Interfaces: Electrodeposition without Electrodes. *J. Electroanal. Chem.* **2000**, *488* (2), 99–109. https://doi.org/10.1016/S0022-0728(00)00185-6.

(36)   Hotta, H.; Akagi, N.; Sugihara, T.; Ichikawa, S.; Osakai, T. Electron-Conductor Separating Oil-Water (ECSOW) System: A New Strategy for Characterizing Electron-Transfer Processes at the Oil/Water Interface. *Electrochem. commun.* **2002**, *4* (5), 472–477. https://doi.org/10.1016/S1388-2481(02)00343-0.

(37)   Hotta, H.; Ichikawa, S.; Sugihara, T.; Osakai, T. Clarification of the Mechanism of Interfacial Electron-Transfer Reaction between Ferrocene and Hexacyanoferrate(III) by Digital Simulation of Cyclic Voltammograms. *J. Phys. Chem. B* **2003**, *107* (36), 9717–9725. https://doi.org/10.1021/jp035058p.

(38)   Gamero-Quijano, A.; Molina-Osorio, A. F.; Peljo, P.; Scanlon, M. D. Closed Bipolar Electrochemistry in a Four-Electrode Configuration. *Phys. Chem. Chem. Phys.* **2019**, *21* (19), 9627–9640. https://doi.org/10.1039/C9CP00774A.

(39)   Tomaszewski, L.; Reymond, F.; Brevet, P. F.; Girault, H. H. Facilitated Ion Transfer across Oil|water Interfaces. Part III. Algebraic Development and Calculation of Cyclic Voltammetry Experiments for the Formation of a Neutral Complex. *J. Electroanal. Chem.* **2000**, *483* (1), 135–143. https://doi.org/10.1016/S0022-0728(00)00013-9.

(40)   Lagger, G.; Carrupt, P.; Girault, H. H. Facilitated Ion Transfer Reactions across Oil Water Interfaces Part II . Use of the Convoluted Current for the Calculation of the Association Constants and for an Amperometric Determination of the Complexes. *J. Electroanal. Chem.* **1998**, *451*, 59–76. https://doi.org/10.1016/S0022-0728(97)00428-2.

(41)   Reymond, F.; Carrupt, P.-A.; Girault, H. H. Facilitated Ion Transfer Reactions across Oil|water Interfaces. Part I. Algebraic Development and Calculation of Cyclic Voltammetry Experiments for Successive Complex Formation. *J. Electroanal. Chem.* **1998**, *449* (1–2), 49–65. https://doi.org/10.1016/S0022-0728(97)00430-0.

(42)   Peljo, P.; Smirnov, E.; Girault, H. H. Heterogeneous versus Homogeneous Electron Transfer Reactions at Liquid–Liquid Interfaces: The Wrong Question? *J. Electroanal. Chem.* **2016**, *779*, 187–198. https://doi.org/10.1016/j.jelechem.2016.02.023.

(43)   Suárez-Herrera, M. F.; Cazade, P. A.; Thompson, D.; Scanlon, M. D. Monitoring Transient Changes in the Structure of Water at a Polarised Liquid-Liquid Interface Using Electrocapillary Curves. *Electrochem. commun.* **2019**, *109* (October), 106564. https://doi.org/10.1016/j.elecom.2019.106564.

(44)   Massonnet, N.; Carella, A.; Jaudouin, O.; Rannou, P.; Laval, G.; Celle, C.; Simonato, J. P. Improvement of the Seebeck Coefficient of PEDOT:PSS by Chemical Reduction Combined with a Novel Method for Its Transfer Using Free-Standing Thin Films. *J. Mater. Chem. C* **2014**, *2* (7), 1278–1283. https://doi.org/10.1039/c3tc31674b.

(45)   Łapkowski, M.; Proń, A. Electrochemical Oxidation of Poly(3,4-Ethylenedioxythiophene) - `in Situ' Conductivity and Spectroscopic Investigations. *Synth. Met.* **2000**, *110* (1), 79–83. https://doi.org/10.1016/S0379-6779(99)00271-4.

(46)   Garreau, S.; Louarn, G.; Buisson, J. P.; Froyer, G.; Lefrant, S. In Situ Spectroelectrochemical Raman Studies of Poly(3,4-Ethylenedioxythiophene) (PEDT). *Macromolecules* **1999**, *32* (20), 6807–6812. https://doi.org/10.1021/ma9905674.

(47)   Garreau, S.; Duvail, J. L.; Louarn, G. Spectroelectrochemical Studies of Poly(3,4-Ethylenedioxythiophene) in Aqueous Medium. *Synth. Met.* **2002**, *125* (3), 325–329. https://doi.org/10.1016/S0379-6779(01)00397-6.

(48)   Bubnova, O.; Khan, Z. U.; Malti, A.; Braun, S.; Fahlman, M.; Berggren, M.; Crispin, X. Optimization of the Thermoelectric Figure of Merit in the Conducting Polymer Poly(3,4-Ethylenedioxythiophene). *Nat. Mater.* **2011**, *10* (6), 429–433. https://doi.org/10.1038/nmat3012.

(49)   Shi, W.; Zhao, T.; Xi, J.; Wang, D.; Shuai, Z. Unravelling Doping Effects on PEDOT at the Molecular Level: From Geometry to Thermoelectric Transport Properties. *J. Am. Chem. Soc.* **2015**, *137* (40), 12929–12938. https://doi.org/10.1021/jacs.5b06584.

(50)   Marquez, A. V.; Mcevoy, N. Organic Electrochemical Transistors (OECTs) toward Flexible and Wearable Bioelectronics. *Molecules* **2020**, *25* (22), 5288. https://doi.org/10.3390/molecules25225288.

(51)   Zotti, G.; Zecchin, S.; Schiavon, G.; Groenendaal, L. B. Conductive and Magnetic Properties of 3,4-Dimethoxy- and 3,4-Ethylenedioxy-Capped Polypyrrole and Polythiophene. *Chem. Mater.* **2000**, *12* (10), 2996–3005. https://doi.org/10.1021/cm000400l.

(52)   Zotti, G.; Zeccjhin, S.; Schiavon, G.; Louwet, F.; Groenendaal, L.; Crispin, X.; Osikowicz, W.; Salaneck, W.; Fahlman, M. Electrochemical and XPS Studies toward the Role of Monomeric and Polymeric Sulfonate Counterions in the Synthesis, Composition, and Properties of Poly(3,4-Ethylenedioxythiophene). *Macromolecules* **2003**, *36* (9), 3337–3344. https://doi.org/10.1021/ma021715k.

(53)   Piradashvili, K.; Alexandrino, E. M.; Wurm, F. R.; Landfester, K. Reactions and Polymerizations at the Liquid-Liquid Interface. *Chem. Rev.* **2016**, *116* (4), 2141–2169. https://doi.org/10.1021/acs.chemrev.5b00567.

(54)   Booth, S. G.; Dryfe, R. A. W. Assembly of Nanoscale Objects at the Liquid/Liquid Interface. *J. Phys. Chem. C* **2015**, *119* (41), 23295–23309. https://doi.org/10.1021/acs.jpcc.5b07733.

(55)   Scanlon, M. D.; Smirnov, E.; Stockmann, T. J.; Peljo, P. Gold Nanofilms at Liquid-Liquid Interfaces: An Emerging Platform for Redox Electrocatalysis, Nanoplasmonic Sensors, and Electrovariable Optics. *Chem. Rev.* **2018**, *118* (7), 3722–3751. https://doi.org/10.1021/acs.chemrev.7b00595.

(56)   Poltorak, L.; Gamero-Quijano, A.; Herzog, G.; Walcarius, A. Decorating Soft Electrified Interfaces: From Molecular Assemblies to Nano-Objects. *Appl. Mater. Today* **2017**, *9*, 533–550. https://doi.org/10.1016/j.apmt.2017.10.001.